JACS
JOURNAL OF THE AMERICAN CHEMICAL SOCIETY
Article
pubs.acs.org/JACS

Efficient Reactivation of p53 in Cancer Cells by a Dual MdmX/Mdm2 Inhibitor

Lingyun Qin,[†] Fei Yang,[†] Cindy Zhou,[‡] Yao Chen,[†] Huashan Zhang,[†] and Zhengding Su*[,†,‡,§]

[†]Department of Biotechnology and Collaborative Innovation Center for Industrial Fermentation, Hubei University of Technology, Wuhan 430068, China

[‡]Amersino Biodevelop Inc., Waterloo, Ontario N2L 3G1, Canada

[§]Department of Structural Biology, St. Jude Children's Research Hospital, Memphis, Tennessee 38105, United States

Supporting Information

ABSTRACT: The aberrant interaction between p53 and Mdm2/MdmX is an attractive target for cancer drug discovery because the overexpression of Mdm2 and/or MdmX ultimately impairs the function of p53 in approximately half of all human cancers. Recent studies have shown that inhibition of both Mdm2 and MdmX is more efficient than that of a single target in promoting cellular apoptosis in cancers. In this study, we demonstrate that a dual small-molecule antagonist of Mdm2/MdmX can efficiently reactivate the p53 pathway in model cancer cells overexpressing MdmX and/or Mdm2. The dual antagonist was rationally designed based on segmental mutational analysis of the N-terminal domain of MdmX and the crystal structure of the N-terminal domain of Mdm2 in complex with nutlin-3a (an Mdm2-specific inhibitor). The current work establishes a small molecule therapeutic candidate that targets cancers overexpressing Mdm2 and/or MdmX.

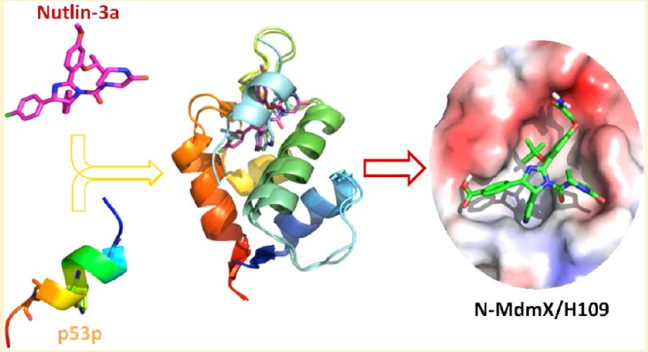

INTRODUCTION

Direct gene alterations of p53 or the binding of Mdm2 and MdmX to the p53 transactivation domain are two alternative mechanisms causing the inactivation of p53 function and tumor survival.[1−3] The elevated expression of Mdm2 and/or MdmX not only accounts for nearly half of all cancers that retain wild-type p53 but also highly correlates with high-grade, late-stage, and more resistant tumors.[3,4] Therefore, reactivation of p53 in wild-type p53-expressing tumors through the release of its physical interaction with Mdm2 and MdmX has become the focus of cancer drug discovery.[3,5]

By now, many small-molecule inhibitors of Mdm2 have been discovered based on combinatorial chemistry and medicinal chemistry.[6] These inhibitors promote p53-mediated cell cycle arrest, apoptosis, and tumor regression in cancer cells overexpressing Mdm2. One of these promising Mdm2 inhibitors is nutlin-3a, which is currently under clinical investigation.[1,7] Although the structures of MdmX and Mdm2 are highly similar, the existing Mdm2 inhibitors exhibit relatively weak binding affinity for the MdmX protein, leading to only marginal induction of apoptosis in tumor cell lines overexpressing MdmX.[8−10] Conversely, recent studies have confirmed that the inhibition of both Mdm2 and MdmX in cancer cells expressing wild-type p53 can activate p53 more strongly than agents that only antagonize Mdm2 activity.[11−13] Thus, to achieve full reactivation of p53 in cancer cells, it is necessary to apply a therapeutic treatment that is dual-specific to disrupt the interaction between p53 and its negative regulators Mdm2 and MdmX. It has recently been made progress for designing dual inhibitors of Mdm2 and MdmX with different rationales that either inhibit both proteins[14,15] or induce the dimerization of Mdm2 and MdmX.[12]

In a cancer cell expressing wild-type p53, p53 activity is often impaired by the interaction of its 15-amino acid transactivation domain (p53p) with the N-terminal domains of Mdm2 and MdmX (referred to hereafter as N-Mdm2 and N-MdmX, respectively). In this study, we compared the ligand binding behaviors of N-Mdm2 and N-MdmX to p53p and nutlin-3a using segmental mutagenesis, NMR spectrometry, and X-ray crystallography, with the aim of designing a dual inhibitor of Mdm2/MdmX that utilizes the nutlin-3a scaffold.

RESULTS

Segmental Mutation Analysis of N-MdmX. N-MdmX and N-Mdm2 are highly homologous in terms of their amino acid sequences, secondary structural elements, and tertiary conformations (Figure 1a,b). It is notable that there are nine segments of N-MdmX that are significantly different from their counterparts in N-Mdm2 with regards to their physicochemical properties including polarity, hydrophobicity, and backbone flexibility. The isolated p53 transactivation domain (p53p) can

Received: September 14, 2014
Published: December 2, 2014

   dx.doi.org/10.1021/ja509223m | J. Am. Chem. Soc. 2014, 136, 18023−18033

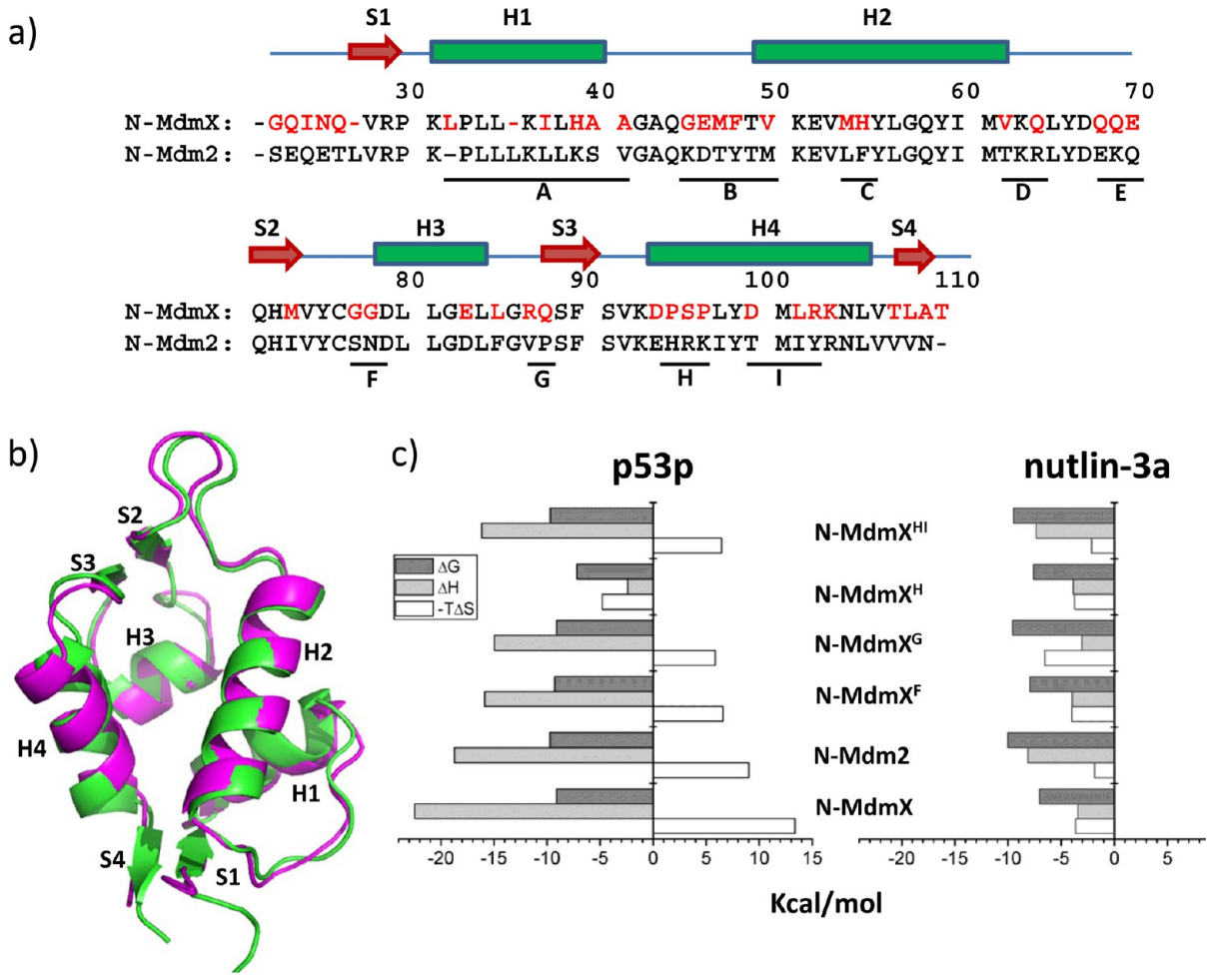

Figure 1. Segmental mutation analysis of the binding affinity of N-MdmX and N-Mdm2 for p53p. (a) Amino acid sequence alignment of N-MdmX and N-Mdm2. The sequences were annotated according to the translated products of their cDNAs. Their secondary elements are depicted based on the structure of the N-MdmX/p53p complexes (3dab.pdb). The symbols S and H denote β-sheet and α-helical structures, respectively. Nine different segments between N-MdmX and N-Mdm2 are marked alphabetically from A to I. (b) N-MdmX and N-Mdm2 showed similar tertiary structures (green: N-Mdm2, 1ycr.pdb and magenta: N-MdmX, 3dab.pdb). (c) The thermodynamic signatures of N-MdmX, N-Mdm2, and N-MdmX mutants binding to p53p (left) and nutlin-3a (right) were compared in pairs.

Table 1. Segmental Mutation Analysis of N-MdmX Binding Affinities for p53p and Nutlin-3a[a]

protein	segment in N-MdmX	substituted segment from N-Mdm2	$K_{d,\ p53p}$ (μM)	$K_{d,\ nutlin\text{-}3a}$ (μM)
N-Mdm2	–	–	0.13 ± 0.02	0.019 ± 0.004
N-MdmX	–	–	0.42 ± 0.03	6.5 ± 0.3
N-MdmX^{A}	^{32}LPLL-KILHAA^{41}	^{32}PLLLKLLKS^{41}	0.48 ± 0.02	8.6 ± 0.4
N-MdmX^{B}	^{44}GEMFT^{50}V	^{44}KDTYT^{50} M	0.43 ± 0.02	6.5 ± 0.3
N-MdmX^{C}	^{54} M^{55}H	^{54}L^{55}F	0.45 ± 0.03	7.7 ± 0.4
N-MdmX^{D}	^{62}VK^{64}Q	^{62}TK^{64}R	0.49 ± 0.02	5.6 ± 0.3
N-MdmX^{E}	^{68}QQ^{70}K	^{68}EK^{70}Q	0.51 ± 0.03	8.4 ± 0.4
N-MdmX^{F}	^{77}G^{78}G	^{77}S^{78}N	0.25 ± 0.01	1.5 ± 0.8
N-MdmX^{G}	^{87}R^{88}Q	^{87}V^{88}P	0.53 ± 0.02	0.064 ± 0.003
N-MdmX^{H}	^{95}PS^{97}P	^{95}HR^{97}K	5.3 ± 0.25	2.7 ± 0.12
N-MdmX^{I}	^{100}DMLR^{104}K	^{100}TMIY^{104}R	0.44 ± 0.02	7.5 ± 0.38
N-MdmX^{HI}	^{96}PSPLYDMLR^{104}K	^{95}HRKIYTMIY^{104}R	0.16 ± 0.09	0.11 ± 0.06

[a]The data are expressed as the average of three replicates with standard derivation error.

bind to N-MdmX and N-Mdm2 with K_d values of 0.42 and 0.13 μM, respectively (Table 1). In contrast, N-MdmX and N-Mdm2 exhibit distinct binding affinities to nutlin-3a with K_d values of 6.5 and 0.019 μM, respectively. Interestingly, even though nutlin-3a shows a weak affinity for MdmX, this molecule was shown to be effective at killing cancer cells in models of cancer caused by MdmX.[16]

We sought to investigate how the nine segments of N-MdmX differentiate the binding affinities of N-MdmX from N-Mdm2 for p53p and nutlin-3a. A series of mutants was constructed by

dx.doi.org/10.1021/ja509223m | J. Am. Chem. Soc. 2014, 136, 18023−18033

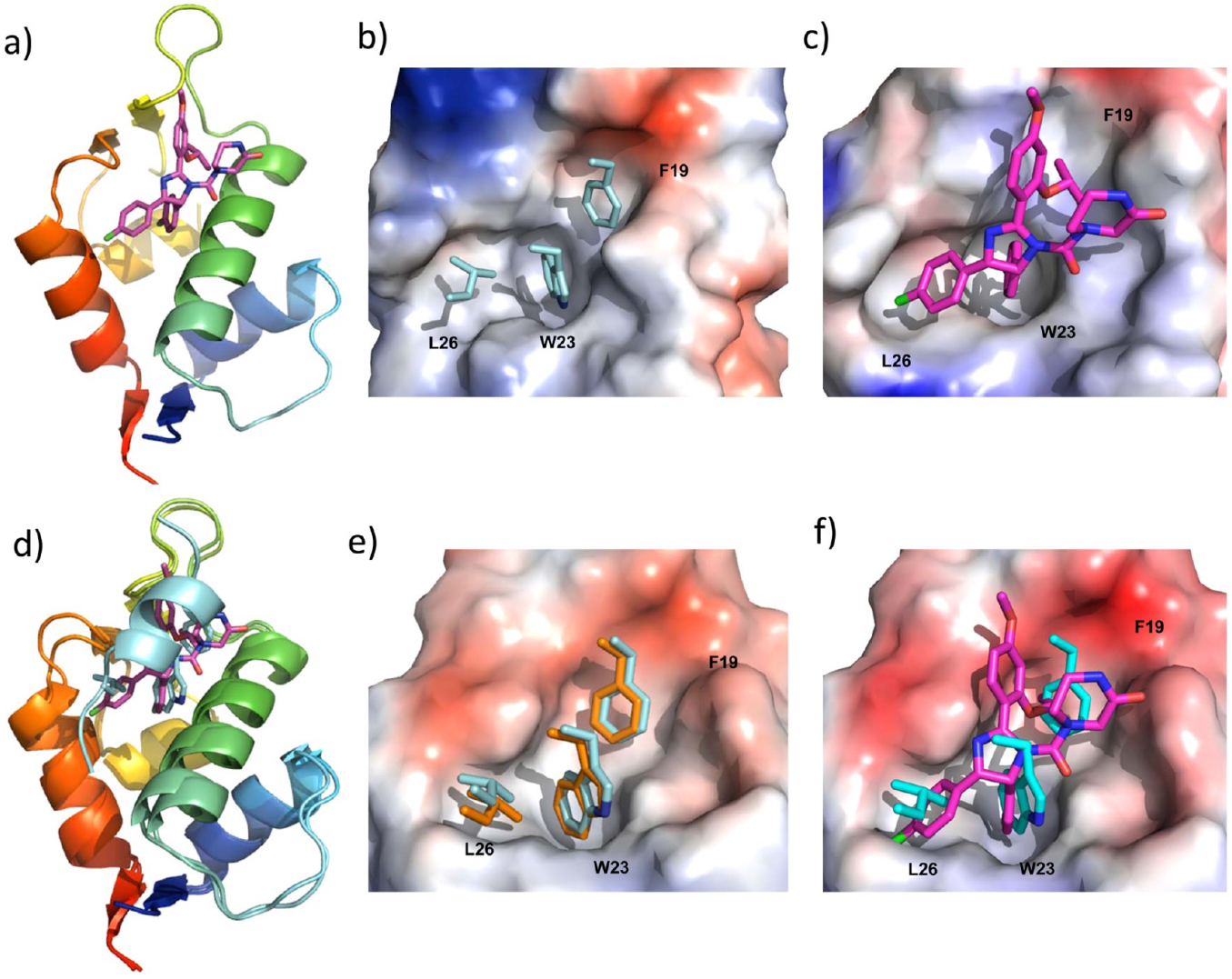

Figure 2. Comparison of the binding surfaces of N-Mdm2 and N-MdmX to p53p and nutlin-3a. (a) An X-ray crystal structure of N-Mdm2 in complex with nutlin-3a was obtained at 1.3 Å in this work. (b) Three binding pockets on N-Mdm2 were defined by adapting to three key residues of p53p, L19, W23, and F26 (1ycr.pdb). (c) The p53p-binding surface on N-Mdm2 changed upon nutlin-3a binding. (d) Nutlin-3a on N-Mdm2 was compared with p53p on N-MdmX (magenta: nutlin-3a; cyan: p53p). (e) The L26 residue of p53p showed a different configurations on the surfaces of N-Mdm2 and N-MdmX (cyan: p53p on Mdm2; orange: p53p on N-MdmX). (f) Nutlin-3a was docked on the p53p binding surface on N-MdmX.

substituting each segment in N-MdmX with its counterpart from N-Mdm2, one at a time. The resulting nine single-segmental mutants were evaluated for their binding affinities for p53p and nutlin-3a by isothermal titration calorimetry (ITC). As summarized in Table 1, the nine mutants exhibited different affinities for p53p and nutlin-3a. Two of these single-segmental replacements yielded significant effects on p53p binding, whereas the others showed no effects. The replacement of segment F (N-MdmX^{F}) significantly enhanced p53p binding compared with the wild-type protein, whereas the replacement of segment H (N-MdmX^{H}) dramatically reduced p53p binding. It is likely that the local conformation of the amino acid sequence around segments F and H has affected the binding of p53p, as the N-MdmX^{F} mutant adopted a relatively rigid sequence from N-Mdm2, whereas in the N-MdmX^{H} mutant, a rigid sequence was replaced with a flexible one.

To determine why the mutant N-MdmX^{H} had a reduced binding affinity for p53p, which was unexpected, we replaced the adjacent segment on helix 4 in N-MdmX^{H} with its counterpart from N-Mdm2 to generate a double segmental mutant (N-MdmX^{HI}). As indicated in Table 1, this double mutation in N-MdmX^{HI} was able to compensate for the affinity loss in the N-MdmX^{H} mutant and showed almost comparable binding affinity to that of N-MdmX. This result suggests that the amino acid sequences from segments F, H, and I might play an important role in determining the p53p binding affinity of N-MdmX and N-Mdm2.

Compared with p53p binding, these segmental replacements showed completely different effects on nutlin-3a binding. The mutations in N-MdmX^{F} and N-MdmX^{H} enhanced nutlin-3a binding in 4.3- and 2.4-fold, respectively, compared with N-MdmX. Notably, the mutation in segment G (N-MdmX^{G}), which resulted in no effect on p53p binding, enhanced nutlin-3a binding more than 100-fold. Like p53p, nutlin-3a exhibited enhanced binding affinity in the double mutant N-MdmX^{HI}. Based on these observations, it is likely that N-MdmX and N-Mdm2 employ different mechanisms for recruiting nutlin-3a and p53p, which are related to the structural conformations of segments F, G, and H.

dx.doi.org/10.1021/ja509223m | J. Am. Chem. Soc. 2014, 136, 18023−18033

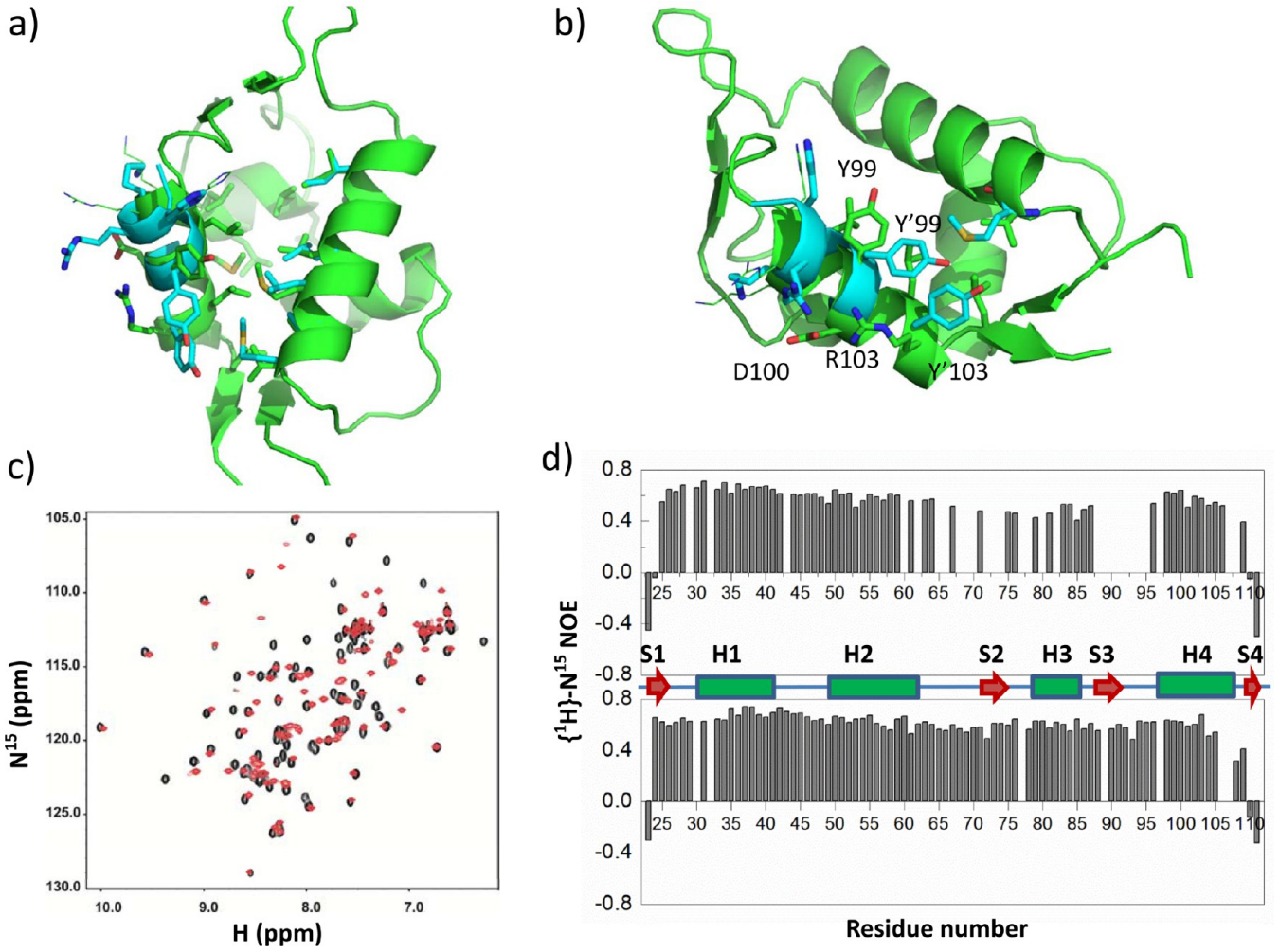

Figure 3. The conformational difference between N-MdmX and N-Mdm2 lies in their H4 helices. (a) The ligand binding surfaces of N-MdmX (green) are formed by the hydrophobic packing from helices H2, H3, and H4. The side chains of segment H (^{95}HR^{97}K) of N-Mdm2 were presented as thin sticks, whereas segment H in mutant N-MdmX^{H} is presented as a thick stick (cyan). The mutation in segment H in the N-MdmX^{H} mutant may result in an inability to the N-terminal conformation of helical H4 into that of its counterpart in N-Mdm2. (b) The hydrophobic interaction between the C-terminus of helix H4 (Y′99, Y′103, L′101, and L′106) with helix H2 tightened the N-Mdm2 conformation, whereas the salt bridge between D100 and R103 in N-MdmX may cause the p53p binding surface to become more open to the solvent environment. (c) The ^{15}N−^{1}H HSQC NMR spectrum of N-MdmX in complex with nutlin-3a (red) was compared with that of N-Mdm2 in complex with nutlin-3a (black). (d) The ^{15}N−^{1}H heteronuclear NOE experiments revealed that the backbone dynamics of N-MdmX (top panel) and N-Mdm2 (bottom panel) were significantly different from each other when complexed with nutlin-3a.

Structural Comparison Between N-Mdm2/Nutlin-3a Complexes and N-MdmX/p53p Complexes. To identify a nutlin-3a scaffold-based analog that targets both Mdm2 and MdmX, we sought to determine the structures of N-Mdm2 and N-MdmX complexed with nutlin-3a. After high-throughput screening for crystallization conditions and further optimization, we were able to obtain a high-resolution X-ray crystal structure of the N-Mdm2/nutlin-3a complex at 1.3 Å (Figure 2a), although our N-MdmX/nutlin-3a complex suffered difficulties in crystallization. Nevertheless, we determined the NMR structure of N-MdmX complexed with a nutlin-3a analog (SJ298).[17] These structural data should provide valuable information to understand the structural mechanism of the interactions of N-MdmX and N-Mdm2 with small molecules.

Our crystal structure revealed that the principal features of the p53p binding surface on N-Mdm2 (Figure 2b, 1ycr.pdb[18]) were preserved during nutlin-3a binding (Figure 2c). The protein surface had a relatively deep hydrophobic pocket that was primarily filled by three p53p side chains (Phe19, Trp23, and Leu26), which were therefore called the F19, W23, and L26 binding pockets, respectively. However, the surface of N-Mdm2 was obviously altered when it was bound to nutlin-3a rather than p53p. These major changes occurred at the F19 and L26 binding pockets (Figure 2c vs 2b). The F19 binding pocket widened, whereas the L26 binding pocket narrowed, forming a hydrophobic surface for docking a chloro group of nutlin-3a. We also observed that the His95 residue of N-Mdm2 interacted with nutlin-3a (data not shown), mimicking the interaction between p53p and the His95 residue of N-Mdm2.[19]

The interaction of nutlin-3a with the N-Mdm2 surface provides a valuable model to predict the interaction of small molecules with N-MdmX. The N-Mdm2 conformation in the N-Mdm2/nutlin-3a complex showed very similar secondary and tertiary structural characteristics to those of N-MdmX complexed with p53p (3dba.pdb, Figure 2d). One interesting observation was that the F19 binding pocket for nutlin-3a on N-Mdm2 was very similar to that observed on N-MdmX complexed with p53p (Figure 2c vs 2e). Conversely, when

dx.doi.org/10.1021/ja509223m | J. Am. Chem. Soc. 2014, 136, 18023−18033

a)

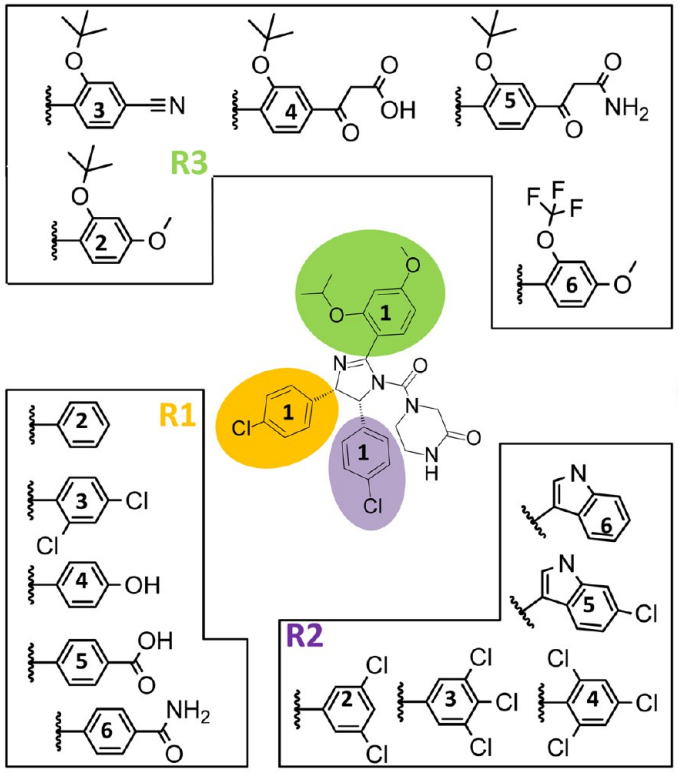

b)

CPD	Group			K_d, (μM)	
	R1	R2	R3	N-MdmX	N-Mdm2
nutlin-3a	1	1	1	6.5 ± 0.32	0.019±0.004
p53p	-	-	-	0.42 ± 0.03	0.13 ± 0.02
H206	2	3	4	0.27 ± 0.07	0.046± 0.007
H135	4	2	6	0.27 ± 0.07	0.17 ± 0.01
H181	3	2	3	0.24 ± 0.06	0.025± 0.004
H077	5	2	5	0.19 ±0.06	0.35 ± 0.01
H196	5	6	5	0.089±0.005	0.34 ± 0.02
H109	5	5	5	0.027±0.004	0.006 ± 0.001

c) d)

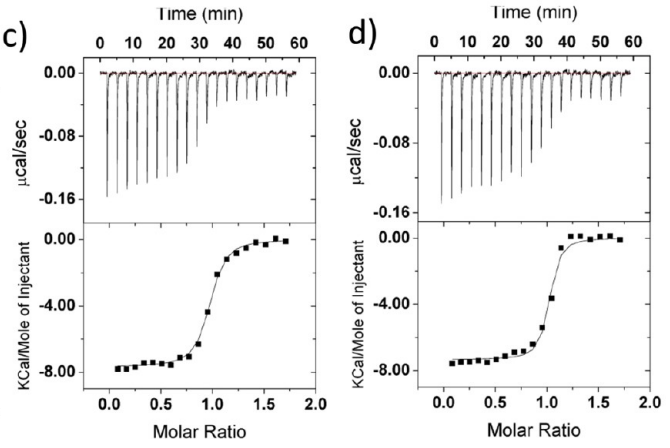

Figure 4. A dual Mdm2/MdmX inhibitor was obtained by screening a structural biology-based combinatorial library of nutlin-3a analogs. (a) A combinatorial library was constructed by focusing on three key functional groups, R_1, R_2, and R_3, of the nutlin-3a scaffold. The annotation of each functional group originated from the nutlin-3a moiety. (b) Six primary compounds were selected by screening the library at IC_{50} < 300 nM, and compound H109 was identified as a promising dual inhibitor that bound to both MdmX and Mdm2. (c) Thermodynamic profiles describing the heat flow over the course of N-MdmX (left) and N-Mdm2 (right) titrated with compound H109 were fitted to a one-site binding model to obtain the values for stoichiometry (n), the binding constant (K_d) and enthalpy (ΔH).

comparing p53p binding on N-MdmX and N-Mdm2, one found that two of the three key residues of p53p, Phe19, and Trp23 are positioned in the same configuration, suggesting that the F19 and W23 binding pockets on N-MdmX should be able to accommodate the corresponding functional groups of nutlin-3a. However, the configuration of Leu26 residue of p53p is shifted approximately 0.6 Å (Figure 2e), caused by the open and closed positions of Tyr99 on N-Mdm2 and N-MdmX, respectively,[19] when the p53p binds to N-MdmX and N-Mdm2, respectively. This observation indicated that the L26 binding pockets are flexible in N-MdmX and N-Mdm2. The W23 binding pocket also becomes shallower in the N-MdmX/p53p complex than N-Mdm2 complexed with p53p (Figure 2b,e). Using a computational docking analysis, we found that neither *para*-chloro group of nutlin-3a fit into the W23 and L26 binding pockets on the p53p binding surface (Figure 2f). Therefore, it is likely that the W23 and L26 binding pockets on MdmX are too flexible to have sufficient interactions with proven Mdm2 inhibitors, particularly the nutlin compounds, as observed using standard docking procedures for mimicking nutlin/MdmX interactions.[20] This flexibility could also explain why nutlin-3a exhibited a weak binding affinity for N-MdmX. Thus, nutlin-3a, as a specific inhibitor of the Mdm2-p53 interaction, has not been optimized for binding to N-MdmX.

Dynamic Characteristics of the Binding Pockets in N-Mdm2 and N-MdmX. The hydrophobic residues from the three helical elements (H2, H3, and H4, Figure 3a) heavily contribute to the formation of W23 and L26 binding pockets in N-Mdm2 and N-MdmX. These binding pockets are closed by the hydrophobic interactions between the C-terminal residues of the H4 helix (i.e., Y′99, Y′103, L′101, and L′106) and the H2 helix (Figure 3a). A salt bridge between D100 and R103 on the H4 helix of N-MdmX exposes its binding surface to the solvent environment, unlike N-Mdm2 (Figure 3b). In NMR experiments, we found that when N-MdmX was complexed with nutlin-3a, its H2 and H4 helices were much more flexible than their counterparts in the N-Mdm2/nutlin-3a complex. All the resonance peaks could be assigned in the N^{15}–H^1 HSQC NMR spectrum for N-Mdm2 in the free form, whereas only 62 out of 89 residues could be assigned in the N-MdmX spectrum. The missing peaks were mainly located in the region between Lys64 and Lys94 in between H2 and H4 helices. Many NMR resonance peaks in the ^{15}N–^1H HSQC spectrum of N-MdmX remained missing from these regions, even in the complex with nutlin-3a (Figure 3c). Upon nutlin-3a binding, only three new resonance peaks appeared for residues Met61, Asp67, and Leu81. Furthermore, our heteronuclear Overhauser effect (NOE) experiments on the complexes confirmed that the region in between Lys64 and Lys94 of N-MdmX was very flexible, even when complexed with nutlin-3a, compared with the N-Mdm2/nutlin-3a complex (Figure 3d), which was related to segments D, E, F, and G (Figure 1a). Considering current

dx.doi.org/10.1021/ja509223m | J. Am. Chem. Soc. 2014, 136, 18023−18033

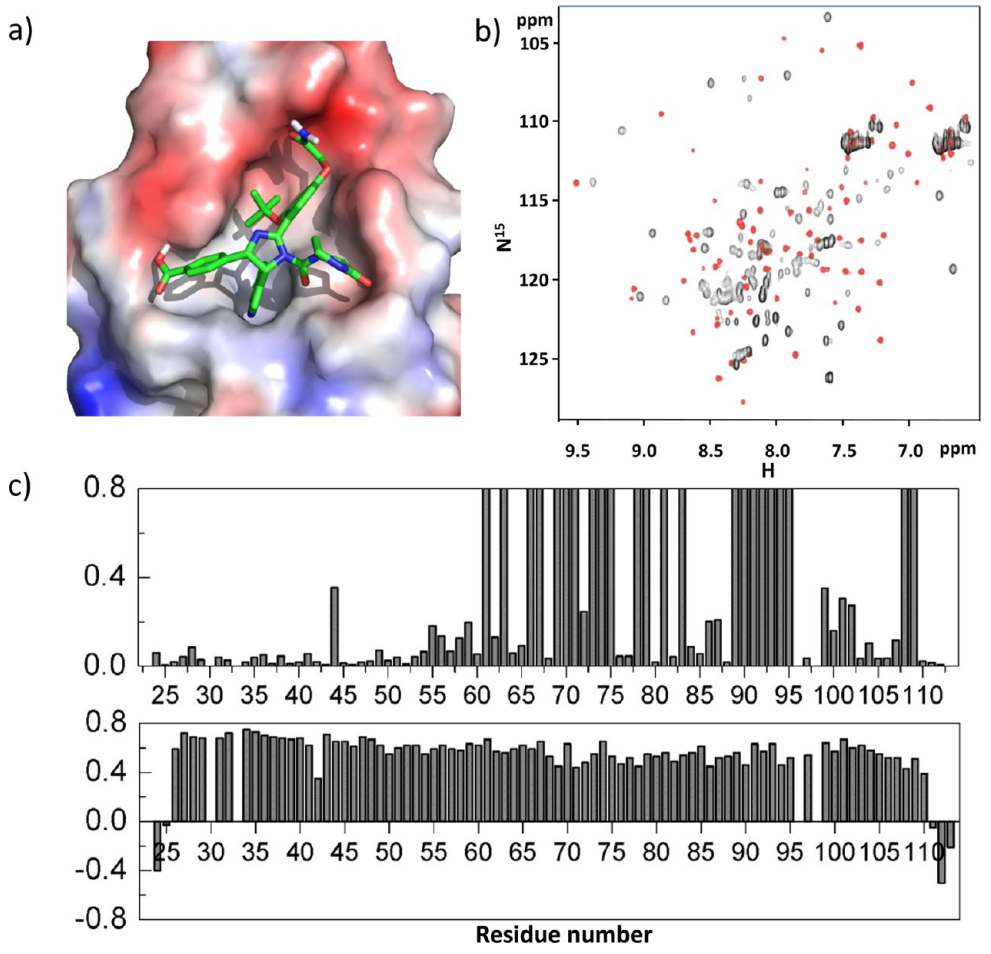

Figure 5. Molecular docking and NMR characterization of the interaction between compound H109 and N-MdmX. (a) Molecular docking experiments suggested that compound H109 could bind to the p53 binding pocket of N-MdmX. (b) The $^{15}N-^{1}H$ HSQC NMR spectrum of N-MdmX titrated with the compound in a ratio of 1:2 (red) compared with N-MdmX in free form (black). (c) The compound significantly perturbed the HSQC resonance peaks of N-MdmX (top panel), especially for the region between residues 60 and 97. Additionally, the $^{15}N-^{1}H$ heteronuclear NOE data (bottom panel) revealed that the backbone dynamics of N-MdmX in the same region became significantly more rigid upon compound binding.

and previous structural investigations on N-MdmX and N-Mdm2 interacting with p53p and nutlin-3a, the interactions between p53p and nutlin-3a differ from those of N-MdmX and N-Mdm2 with respect to segments G, H, and I. It was likely that the hydrophobic packing by H2, H3, and H4 helices as well as the rigidity of S2 and S3 sheets and H3 helix cooperated to form different binding surfaces on N-MdmX and N-Mdm2, which determined their binding affinities for p53p and nutlin-3a. Our observations suggested that the development of potent dual inhibitors for MdmX and Mdm2 should be feasible when starting from the nutlin-3a scaffold; in particular, these efforts should focus on enhancement of the hydrophobic packing of H2, H3, and H4 helices as well as the rigidity of S2, S3 sheets and H3 helix.

Rational Design of MdmX/Mdm2 Dual Inhibitors. We next optimized the nutlin-3a scaffold for N-MdmX binding to obtain a dual inhibitor targeting both Mdm2 and MdmX. To achieve this goal, we considered the following combined strategies: (1) enhancing the hydrophobic interactions of the designed compounds with the F19 and W23 binding pockets; (2) reducing the volume of the pharmacophores for the L26 binding pocket and W23 binding pocket; (3) introducing hydrogen bonding between the designed compounds and the binding pockets, as hydrogen bonding has been found to enhance the binding of p53 peptidomimetics and small molecules;[19,21] (4) enhancing the rigidity of S2, S3 sheets and H3 helix as the region between S2 and S3 in the N-MdmX/nutlin-3a complex is significantly more flexible than that in the N-Mdm2/nutlin-3a complex. Therefore, modification of nutlin-3a focused on its three main pharmacophores (R_1, R_2, and R_3 in Figure 4a) to develop nutlin3a-analogs to fit into the p53p binding surface on N-MdmX. The modification of these functional groups in nutlin-3a was strictly limited to the pharmacophores that existed among FDA-approved small-molecule drugs, as assessed through chemoinformatics.[22] Accordingly, a structure-oriented nutlin-3a analog library containing 216 compounds was prepared using combinatory chemistry (Figure 4a).

These compounds were screened for their binding affinities using a fluorescence polarization (FP) assay (see Materials and Methods). Six compounds from the library were found to displace p53p from the N-MdmX/p53p complex with median inhibitory concentration (IC_{50}) values <300 nM. The binding affinities of the six compounds for N-MdmX were further evaluated with ITC to obtain the K_d values (Figure 4b). Three of the six compounds were confirmed to maintain high affinity

dx.doi.org/10.1021/ja509223m | J. Am. Chem. Soc. 2014, 136, 18023−18033

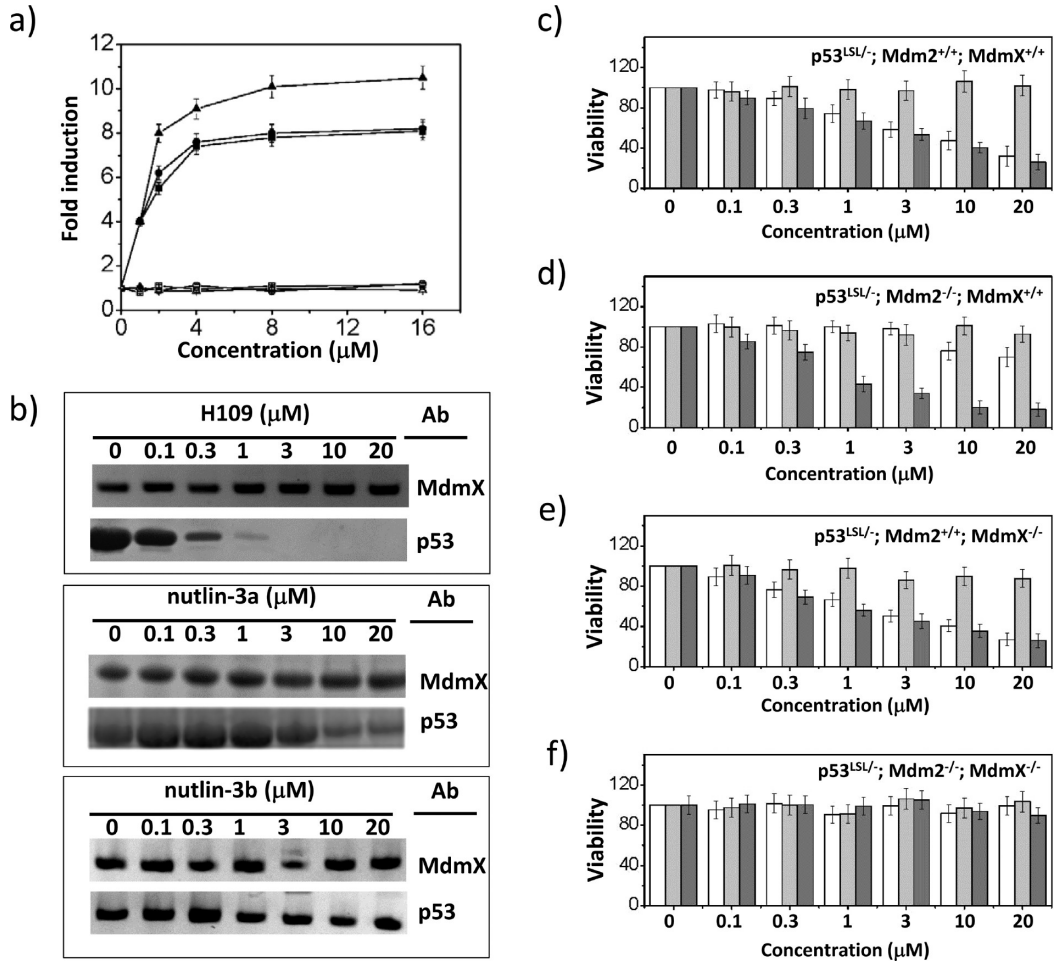

Figure 6. Inhibition of Mdm2/MdmX-p53 binding by compound H109 activates the p53 pathway in cancer cells with wild-type p53. (a) Treatment with compound H109 induced the expression of the p21 gene but not the p53 gene. Solid and open symbols indicate p21 and p53 transcription levels, respectively. Triangle: H460a cell; circle: RKO cell; and square: HCT116 cell. Data were averaged from three replicates. (b) Inhibition of the interaction between N-MdmX and p53 by H109 was assayed using GST pull-down experiments (top panel) in comparison with nutlin-3a (middle panel) and nutlin-3b (bottom panel). N-MdmX and p53 proteins were detected with their antibodies (Ab) on SDS-PAGE gels. (c–f) Cell viability of Cre-infected cells expressing Mdm2 and/or MdmX was significantly influenced by H109 compared with nutlin-3a and nutlin-3b. Empty bar: nutlin-3a (a positive control); gray bar: nutlin-3b (an inactive nutin-3a analog as a negative control); and, dark bar: H109. Reduced cell viability following the addition of H109 was observed in cells expressing both Mdm2 and MdmX (panel c). H109 induced apoptosis in cells lacking either Mdm2 or MdmX. Like nutlin-3a, a significant and dose-dependent decrease in cell number was observed in H109-treated cells lacking MdmX (panel d), and importantly, similar phenomena were also observed in cells lacking Mdm2 (panel e). In contrast, nutlin-3b exhibited no effect on the cell viability for all the tested cells. Cells lacking both Mdm2 and MdmX were largely unaffected by treatment with H109 (panel f). The data represent the mean (±standard deviation) of three independent experiments.

for N-Mdm2. One of these compounds, compound H109, exhibited high affinity for both N-MdmX and N-Mdm2 with K_d values of 27 nM for N-MdmX and 5.7 nM for N-Mdm2 (Figure 4b,d).

Specificity and Dose Response of the Potent Inhibitor. Through molecular docking, compound H109 nicely fits the p53p binding surface on N-MdmX (Figure 5a). A $^{15}N-^{1}H$ HSQC spectrum of N-MdmX in complex with the compound in a molar ratio of 1:2, respectively, generated sharp resonances, compared with those of N-MdmX in the free form (Figure 5b). Upon H109 binding, the flexible region in the N-MdmX backbone became significantly perturbed and rigid (Figure 5c). It was likely that H109 enhanced binding affinity to N-MdmX through multiple modes, including the enhancement of hydrophobic interactions in the W23 and L26 binding pockets and the reduction in backbone dynamics in the region around Gln71 and Val92 residues via the hydrogen bonds introduced.

Compound H109 should be effective only in cells with wild-type p53 and not in cells with transcriptionally inactive p53. To determine whether the inhibition of p53-Mdm2/MdmX binding by H109 could be translated into the activation of the cellular p53 pathway, we treated three cancer cell lines with wild-type p53, HCT116, RKO, and H460a, which were previously used to evaluate nutlin-3a,[7] with H109 for 8 h and monitored the expression of the p53 and p21 genes via real-time polymerase chain reaction (RT-PCR). As indicted in Figure 6a, the transcription of p21 increased in a dose-dependent manner in all cell lines, consistent with the accumulation of its transcriptional activator, p53. By contrast, transcription of the p53 gene itself was unaffected by H109. These data indicated that the compound up-regulated p53 via a post-translational mechanism functioning like nutlin-3a.

dx.doi.org/10.1021/ja509223m | J. Am. Chem. Soc. 2014, 136, 18023–18033

To confirm the specificity of the effect of H109 on MdmX, a GST-N-MdmX fusion protein was used to pull down p53 in vitro in the presence of H109, nutlin-3a, or nutlin-3b. As shown in Figure 6b, H109 significantly inhibited the interaction of N-MdmX with the p53 protein at a concentration of >0.3 μM, whereas nutlin-3a showed a marginal inhibition of the interaction of N-MdmX with p53 until 20 μM of ligand was applied. As expected, nutlin-3b showed no inhibition of the same interaction at the tested ligand concentrations.

To test in vivo whether H109 could induce the p53 pathway by inhibiting MdmX binding to p53, we utilized an Mdm2 or MdmX-deficient mouse embryonic fibroblast (MEF) growth assay. The $p53^{LSL/-}$ MEFs with the indicated genotypes were infected with adeno-GFP-Cre for 12 h to allow Cre-mediated excision of the stop element and subsequent p53 expression according to methods reported previously.[16,23,24] The cells were then exposed to H109, nutlin-3a (the positive control), or nutlin-3b (the negative control) for 48 h, and cell growth/viability was measured using an MTT assay. As a result, reduced cell viability was observed in Cre-infected cells expressing both Mdm2 and MdmX (Figure 6c), and a significant and dose-dependent decrease in cell number was observed in H109-treated cells lacking Mdm2 (Figure 6d) or MdmX (Figure 6e). On the contrary, nutlin-3a exhibited strong inhibition of the cells expressing Mdm2 (Figure 6e), but not those expressing MdmX (Figure 6d). Cells lacking both Mdm2 and MdmX were largely unaffected by this treatment (Figure 6f). Taken together, these results suggested that the nutlin analog-mediated decrease in cell viability was strictly p53-dependent and that compound H109 more specifically affected MdmX than nutlin-3a.

DISCUSSION

In this study, our segmental mutagenesis experiments showed that different amino acid sequences differentiated the binding affinity of nutlin-3a and p53p for N-MdmX and N-Mdm2, which aided our design of a compound library to obtain potent inhibitors of Mdm2/MdmX. Previously, two crystal structures of N-Mdm2 in complex with nutlin compounds were reported, one of which was obtained using a surface entropy reduction mutant ($N\text{-}Mdm2^{E68A+K69A}$, 4hg7.pdb)[25] and another obtained from N-Mdm2 complexed with a nultin-3a analog (two chlorophenyl groups were replaced with bromophenyl groups, 1RV1).[7] The mutant Mdm2 structure and the structures of the wild-type Mdm2 complexed with nutlin-3a share essentially the same features, indicating a compact binding pocket for nutlin-3a. Although detailed structural information on N-MdmX/nutlin-3a complexes is not currently available, comparison of the structures of N-MdmX/p53p and N-Mdm2/p53p complexes as well as the Mdm2/nutlin-3a structures revealed that the binding pocket of nutlin-3a on N-Mdm2 is very similar to the p53-binding pocket on N-MdmX. However, some differences exist between the two pockets. One obvious observation is that in the ligand binding pocket in N-MdmX, the residue Tyr99 (from H2 helix) and the residue Met54 (from H4 helix) block ligand binding when interacting with p53p. Additionally, the N-terminus of N-MdmX H4 helix widens the binding pockets, resulting in two shallow surfaces in the W23 and L26 pockets of N-MdmX that are different from those in N-Mdm2. These features were also observed in the crystallographic structure of N-MdmX complexed with WW298, a weak inhibitor of MdmX designed by Popowicz et al.[26] Taken together, these results indicate possible "cross-talk" between the W23 and L26 binding pockets.[27] Conversely, our ITC data also confirmed that the binding of nutlin-3a to these surfaces on Mdm2 and MdmX exhibited different thermodynamic behaviors. As indicated previously by Popowicz et al.,[28] our data also suggest that there is a high probability that a MdmX-specific inhibitor would exhibit strong affinity for Mdm2. Therefore, our mutational and structural analysis not only explains why antagonists of Mdm2 that mimic the p53 peptide, such as nutlin-3a, ineffectively bind to MdmX, but also provides a rationale for designing inhibitors of both Mdm2/MdmX based on the nutlin-3a scaffold. In this study, we developed a dual-specific MdmX/Mdm2 inhibitor by accounting for the unique structural properties of MdmX as well as the common features of Mdm2/MdmX.

When considering nutlin-3a as a scaffold, our data suggested that an MdmX inhibitor should focus on the enhancement of its interaction with the W23 and L26 surfaces as well as the adjacent region around the N-terminus of helix H4 in N-MdmX. In particular, mimicking the interaction of His95 residue with small molecules should be considered, as it has recently been used to successfully design a new nutlin analog.[21] Importantly, the introduction of hydrogen bonding was determined to be essential for enhancing compound binding in this work. Notably, that the comparison of a previous $N\text{-}Mdm2^{E68A+K69A}$/nutlin-3a structure with the current structure of N-Mdm2/nutlin-3a suggests that the mutation region of segment E in N-MdmX contains sites for introducing hydrogen bonding between small molecules and N-MdmX. Accordingly, a nutlin-3a-based compound library of the dual small-molecule inhibitors of the Mdm2/MdmX-p53 interaction was designed for initial screening, and as a result, a few high-affinity dual inhibitors were identified (Figure 4). Compared with a previous dual Mdm2/MdmX inhibitor that can efficiently inhibit the p53-Mdm2/MdmX interaction by inducing Mdm2/MdmX dimerization,[12] the current inhibitors bind to two targets individually; however, the detailed mechanism needs to be verified through structural investigation.

Inhibition of both Mdm2 and MdmX expression by dual peptide inhibitors and antisense oligonucleotides has been shown to kill tumors caused by overexpressed MdmX.[11,12,29] The dual small-molecule inhibitors of the Mdm2/MdmX-p53 interaction obtained in this work have also been confirmed to exhibit p53-dependent activity in multiple cellular models, implying that their antitumor mechanism is derived from the activation of the p53 pathway. Our work strengthens the notion that reactivating the powerful growth-suppressive and pro-apoptotic activity of p53 by inhibiting Mdm2/MdmX is a promising and valuable strategy for treating cancer, but further investigation is needed to address its true therapeutic potential.

MATERIALS AND METHODS

Cell Lines and Reagents. HCT116, KAO, and H164a cells (ATCC) were cultured in a 37 °C incubator with 5% CO_2 according to ATCC protocols. Nutlin-3a and nutlin-3b were purchased from Sigma (St. Louis, USA). Anti-p53, anti-MdmX, anti-β-actin, antirabbit IgG-HRP, antimouse IgG-HRP, and normal mouse/rabbit IgG were products of Santa Cruz Biotechnology (Santa Cruz, USA). Lipofectamine 2000 was a product of Invitrogen.

Protein Preparation. The genes encoding the p53-binding domain of human MdmX (N-MdmX, amino acids 22−110) and human Mdm2 (N-Mdm2, amino acids 22−110) were synthesized with *E. coli* optimized codons and subcloned into a modified pET28 plasmid (Novagen), in which the thrombin cleavage site was replaced with a TEV protease site. The same N-MdmX DNA fragment was also

subcloned into a pGEX-5P-1 vector (GE) to produce a GST fusion protein. The full length of wild-type p53 DNA was subcloned into the aforementioned the pET vector to produce a HIS-tag fusion protein.

To construct the segmental mutations, the pET28-MdmX plasmid was used as a PCR template. For each mutation, a pair of primers was designed so that the 5′-end sequences matched those in the template. The first batch of PCR reactions was performed individually for each side of the targeted mutation site with one of the T7 universal primers paring with one of the designed mutational primers, followed by PCR purification with a PCR purification kit (Qiagen). The PCR products from the first batch of reactions were used as templates for the second batch of PCR reactions, for which only two T7 universal primers were used. Subsequently, the DNA fragments were treated with restriction enzymes and subcloned into the pET28 vector, which has been pretreated with the same restriction enzymes. All of the mutations were confirmed with DNA sequencing.

Recombinant proteins were prepared in *E. coli* BL21 (*DE3*) cells. Cells were grown in Luria broth and protein expression was induced with 0.4 mM IPTG at 20 °C for 12 h. For heteronuclear NMR experiments, protein samples were uniformly labeled with ^{15}N in M9 minimal medium with BME vitamins (Sigma) containing 2 g/L $(^{15}NH_4)_2SO_4$ and 2 g/L[$^{13}C_6$] glucose as the sole sources of nitrogen and carbon, respectively. Cells were harvested from a 1 L culture by centrifugation at 8000 × *g* for 30 min, resuspended in a lysis buffer and subjected to periodic sonication for 5−6 min. The lysates were cleared by spinning at 100,000 × *g*, and the supernatant was loaded onto a 20 mL Ni-NTA agarose column (Qiagen). If necessary, the His6-tags of the proteins were removed with TEV protease digestion at 4 °C overnight, followed by a second Ni-NTA agarose chromatographic purification. The flow-through was concentrated to 10−12 mL, followed by purification with a S200 gel filtration column (GE). Peak fractions were combined and concentrated to 1 mg/mL, freshly frozen in liquid nitrogen, and kept at −80 °C.

GST-N-MdmX was purified with GST beads and gel exclusion chromatography. Peak fractions were combined and concentrated to 1 mg/mL, freshly frozen in liquid nitrogen, and kept at −80 °C.

ITC. The protein−ligand interactions were characterized using an isothermal titration microcalorimeter, ITC200 (GE Healthcare/MicroCal), at 25 °C. A typical experiment included the injection of 19 aliquots (2.1 μL each) containing approximately 0.2 mM ligand solution into a protein solution of approximately 10−20 μM in the ITC cell (volume approximately 200 μL). An additional set of injections was run in a separate experiment with buffer in the cell instead of the protein solution as a control. Before data analysis, the control values were subtracted from the main experimental data.

The binding isotherms were integrated to give the enthalpy change (ΔH) plotted as a function of the molar ratio of the ligand. When necessary, prior to the integration procedures, the baseline was manually adjusted to minimize the background noise. The initial titration point was always discarded. The ΔH/molar ratio plot was a sigmoidal, representing the fractional saturation of the binding sites by the ligand. The Origin 7.0-based software provided by GE/MicroCal was used for data analysis, and the one set of sites model was used as the basic option. The association constant K_a ($1/K_d$) was determined from the slope of the central linear part of the fractional saturation curve. The Gibbs free energy change (ΔG) and the entropy change (ΔS) were calculated based on the following equations: $\Delta G = -RT\ln K_a = \Delta H - T\Delta S$, where ΔH was derived from the original ΔH/molar ratio plots.

Crystallization and Protein Structure Determination. To prepare protein/ligand complexes for crystallization, frozen N-Mdm2 was thawed and buffer exchanged using a Centricon concentrator (3000 MW cutoff) to 20 mM Tris, pH 7.0, 200 mM NaCl, and 2 mM DTT. The complex was then formed by combining the protein with inhibitor at a molar ratio of 1:3−5, respectively, and allowing overnight incubation at 4 °C, followed by concentrating to 12−15 mg/mL. Crystallization were assessed with Qiagen kits and optimized using the hanging drop vapor diffusion method. The reservoir solution contained 18% saturated ammonium sulfate and 100 mM Tris (pH 7.0). Rectangular crystals grew in 1 week and could be cryopreserved by brief exposure to a solution containing equal volumes of the crystal growth reservoir and 25% ethylene glycol, followed by introduction into liquid nitrogen.

Cryopreserved crystals were transported to beamline X8C at the National Synchrotron Light Source at Brookhaven National Laboratory. The data were collected at 100 K with a Quantum 4 detector (ADSC) at resolution of 1.3 Å and processed using HKL2000. The crystal used for structure solution was in space group C2 with cell dimensions a = 121.21 Å, b = 38.43 Å, c = 67.87 Å and β = 112.34°. Overall, the data set was 98.2% complete, had a redundancy of 3.4, and merged well with R = 0.055. Structure solution was achieved using the program MOLREP from the CCP4 suite and a search model based on the published N-Mdm2 structure (1ycr.pdb).[18] Structure presentations were prepared using PyMol software.

NMR Experiments. All NMR spectra were collected at 25 °C on a Bruker Avance 600 MHz spectrometer equipped with a triple-resonance pulsed-field gradient probe. $^{15}N-^{1}H$ HSQC NMR spectra were recorded in the States-TPPI mode for quadrature detection.[30] All the NMR samples were prepared in a buffer containing 20 mM sodium phosphate, 200 mM NaCl, 2 mM DTT, 0.02% NaN_3, and 95% H_2O/5% D_2O at pH 6.0. Protein samples were prepared through buffer exchange with the NMR buffer. The final concentration of the protein complex was approximately 0.4 mM. All data sets were acquired with 2048 complex points in t_2 and 128 complex points in t_1. All data sets were processed using NMRPipe. Spectral display, assignments, and analysis were performed using the NMRView software package. Time domain data were zero-filled once and apodized with a 90-shifted cosine-squared window function. Solvent suppression was achieved by postacquisition convolution of the time domain data.

The heteronuclear NOE values were measured at 800 MHz for ^{15}N-labeled protein complexed with nutlin-3a using the pulse sequences described by Farrow et al.[31] A 5 s recycle delay was used for the heteronuclear NOE experiment. Steady-state heteronuclear NOE data were obtained in an interleaved manner with and without proton presaturation (3 s). Errors in the heteronuclear NOE values were estimated from the root-mean-square variation of noise in empty regions of the two spectra as previously described.[32]

Preparation of the Combinatorial Library. Synthesis of nutlin analogs was performed using the procedure developed by Davis et al.[33] via the development of a diastereo- and enantioselective bisamidine-catalyzed aryl nitromethane addition to an azomethine. A general procedure to synthesize nutlin-3a analogues is described as follows.

All reactions used 1.1 equiv of nitroalkane in toluene (0.1 M) with a 18−26 h reaction time unless otherwise noted. If the R_1, R_2, or R_3 group contained a carboxyl or amine subgroup, it was protected and deprotected with standard procedures.

The reaction was monitored by LC-MS until conversion was complete. The reaction was quenched with water. The aqueous layer was extracted with dichloromethane. The organic layers were combined, dried over sodium sulfate, and concentrated to give the crude product. Purification was performed on a Waters reverse-phase HPLC (C18 column, mobile phase: water with 0.1% formic acid and methanol with 0.1% formic acid) and was further separated by SFC (OD-H column) in order to give pure enantiomers.

FP Assays. FP assays were conducted in assay buffer containing 10 mM Tris (pH 8.0), 200 mM NaCl, and 0.01% Tween-20. The p53p peptide (amino acids 15−29) was labeled with fluorescein, (fluorescein-GSGSSQETFSDLWKLLPEN, Flu-p53p), and a mutant p53 peptide (fluorescein- GSGSSQETASDLAKLAPEN, Flu-p53p^{AAA}) was used as the negative control.

The FP assays were performed with 15 nM fluorescein and 1 μM N-MdmX. For the N-MdmX/peptide inhibitor assay, nutlin analogs were pre-incubated with the protein for 30 min. Each labeled peptide was then added and incubated for 30 min. FP assays were conducted in 384-well black microplates (Corning). The FP assays were analyzed using an EnVision multilabel plate reader with a 555 nm excitation filter and a 632 nm static and polarized filter. The unlabeled competitor peptide and nutlin-3a were used as positive controls, and the alanine-substituted p53 peptide (p53p^{AAA}) was used as a negative control.

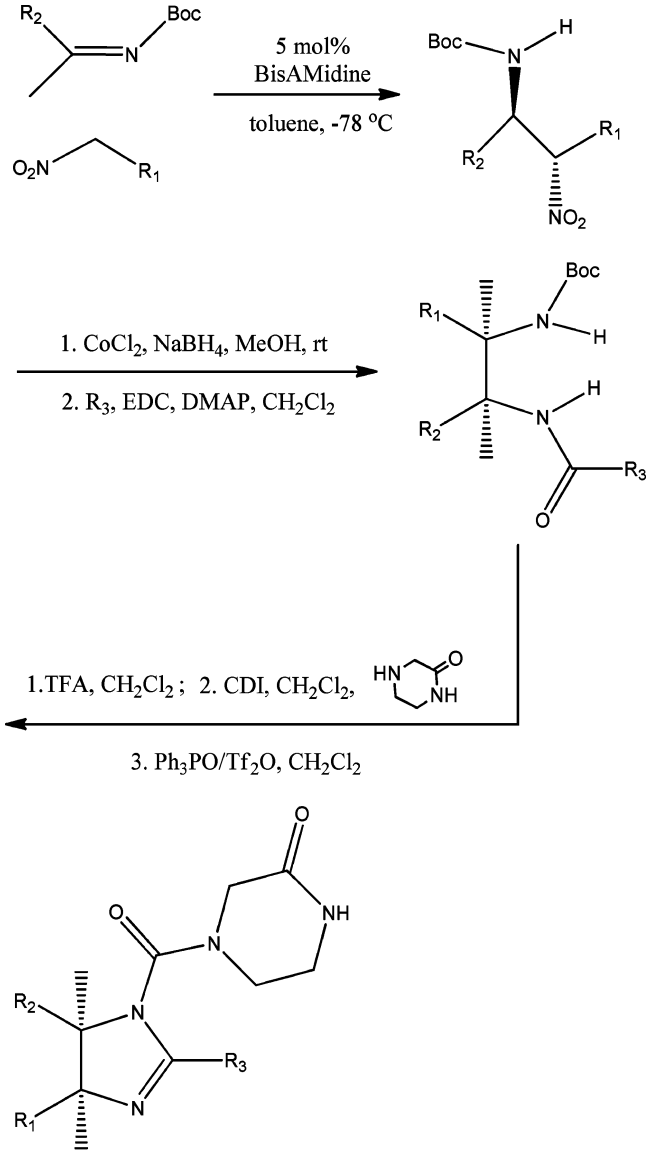

(-)-Nutlin-3a analog

Computational Docking. Potent dual inhibitors selected from the library were generated with ChemBioDraw 13 and further energetically minimized with ChemBio3D (PerkinElmer). The minimized structures were exported in pdb format and manually evaluated using the AutoDock 4 program.[34] The receptor grid box was set directly on the Mdm2 crystal structure obtained in this study after extraction of the included nutlin-3a molecule.

Real-Time PCR. Cancer cells with wild-type p53 (HCT116, RKO, and H460a) were treated with H109 for 8 h, and the change in the level of transcription was measured by quantitative PCR and expressed as fold induction compared with the untreated control. Total RNA was prepared, reverse transcribed, and subjected to real-time PCR assays with the primers for p21 and p53. RT-PCR experiments were performed using the ABI7900HT system (Applied Biosystems). Primers and probes were designed using Primer Express software (Applied Biosystems). TaqMan probes were synthesized with 5′ 6-carboxyfluorescein and 3′ black hole quencher. RNA was prepared using TRIzol reagent, and cDNA was synthesized using the SuperScript system (Invitrogen, Carlsbad, CA).

GST Pull-Down Assays and Western Blotting. A GST pull-down experiment was employed to reconstitute the two-component molecular complexes formed by N-MdmX and p53. GST-N-MdmX bound to glutathione agarose beads incubated with the wild-type p53 protein (1:3 molar ratio) in the binding buffer (50 mM sodium phosphate, pH 6.8) for 2 h at 4 °C in the absence or presence of compound. The beads were washed extensively with the binding buffer, and the samples were boiled for 10 min in the SDS-PAGE sample buffer.

Proteins were separated by SDS-PAGE and electrically transferred to a polyvinylidene difluoride membrane (Millipore, USA). After blocking in 5% skim milk in tris buffered saline (TBS), the membranes were probed with specific primary antibodies overnight at 4 °C, washed three times with TBS-Tween 20, and incubated with HRP-conjugated secondary antibodies at room temperature for 1 h. Then, the membranes were washed with TBS-Tween 20, and the protein bands were visualized using enhanced chemiluminescence (ECL) reagents (Pierce Chemical Co., USA).

MTT Assays. MEF preparation and adenoviral infections were performed in a mouse model according to the procedures described by Laurie et al.[16] All animal studies were performed in accordance with the guidelines approved by the Institutional Animal Care and Use Committee (IACUC). Briefly, the p53 gene in mice was flanked by loxP sites by use of a transcriptional stop element (LSL). The allele was transferred into Mdm2 and/or MdmX-null background. MEFs were prepared from 13-day-old embryos and infected with adeno-Cre-GFP (Vector Development Lab) for 12 h to allow for efficient infection and LSL excision. Cells were grown at 37 °C with 5% CO_2 in Dulbecco's modified eagle medium supplemented with 10% serum, penicillin, and streptomycin. For the proliferation assay, cells were plated at a density of $1 \times 10^4/cm^2$. After 2 h, 1 μL of 100× nutlin-3a analog, nutlin-3a, or nutlin-3b in d_6-dimethyl sulfoxide was added and cells continued to culture for 48 h at 37 °C. The plate was set out for 20 min to reach room temperature, and then 100 μL Cell-Titer-Glo (Promega, USA) was added. The plate was immediately mixed for 2 min and then was placed in a dark drawer for 15 min. The plate contents were read on an Envision 2103 multilabel plate reader (PerkinElmer). Data were processed with MicroCal Origin software (v8.0, MicroCal).

■ ASSOCIATED CONTENT

Ⓢ Supporting Information

There are additional results and discussion on thermodynamic characteristics of segmental mutants binding to p53p and nutlin-3a as well as thermodynamic profiles of N-MdmX mutants in comparison with N-MdmX and N-Mdm2, titrated with p53p and nutlin-3a. This material is available free of charge via the Internet at http://pubs.acs.org.

■ AUTHOR INFORMATION

Corresponding Author

z2su@uwaterloo.ca or zhengding.su@stjude.org

Notes

The authors declare no competing financial interest.

■ ACKNOWLEDGMENTS

We thank Dr. David Duda for his excellent technical assistance. This work was partially funded by the Key Laboratory of Fermentation Engineering (Ministry of Education).

■ REFERENCES

(1) Muller, P. A.; Vousden, K. H. *Nat. Cell Biol.* **2013**, *15*, 2−8.
(2) Cheok, C. F.; Verma, C. S.; Baselga, J.; Lane, D. P. *Nat. Rev. Clin. Oncol.* **2011**, *8*, 25−37.
(3) Wade, M.; Li, Y. C.; Wahl, G. M. *Nat. Rev. Cancer* **2013**, *13*, 83−96.
(4) Macchiarulo, A.; Giacche, N.; Carotti, A.; Moretti, F.; Pellicciari, R. *Med. Chem. Commun.* **2011**, *2*, 455−465.
(5) Popowicz, G. M.; Domling, A.; Holak, T. A. *Angew. Chem., Int. Ed. Engl.* **2011**, *50*, 2680−2688.

(6) Zak, K.; Pecak, A.; Rys, B.; Wladyka, B.; Domling, A.; Weber, L.; Holak, T. A.; Dubin, G. *Expert. Opin. Ther. Pat.* **2013**, *23*, 425−448.
(7) Vassilev, L. T.; Vu, B. T.; Graves, B.; Carvajal, D.; Podlaski, F.; Filipovic, Z.; Kong, N.; Kammlott, U.; Lukacs, C.; Klein, C.; Fotouhi, N.; Liu, E. A. *Science* **2004**, *303*, 844−848.
(8) Carrillo, A. M.; Bouska, A.; Arrate, M. P.; Eischen, C. M. *Oncogene* **2014**, DOI: 10.1038/onc.2014.27.
(9) Kruse, J. P.; Gu, W. *Cell* **2009**, *137*, 609−622.
(10) Huang, L.; Yan, Z.; Liao, X.; Li, Y.; Yang, J.; Wang, Z. G.; Zuo, Y.; Kawai, H.; Shadfan, M.; Ganapathy, S.; Yuan, Z. M. *Proc. Natl. Acad. Sci. U.S.A* **2011**, *108*, 12001−12006.
(11) Graves, B.; Thompson, T.; Xia, M.; Janson, C.; Lukacs, C.; Deo, D.; Di Lello, P.; Fry, D.; Garvie, C.; Huang, K. S.; Gao, L.; Tovar, C.; Lovey, A.; Wanner, J.; Vassilev, L. T. *Proc. Natl. Acad. Sci. U.S.A* **2012**, *109*, 11788−11793.
(12) Chang, Y. S.; Graves, B.; Guerlavais, V.; Tovar, C.; Packman, K.; To, K. H.; Olson, K. A.; Kesavan, K.; Gangurde, P.; Mukherjee, A.; Baker, T.; Darlak, K.; Elkin, C.; Filipovic, Z.; Qureshi, F. Z.; Cai, H.; Berry, P.; Feyfant, E.; Shi, X. E.; Horstick, J.; Annis, D. A.; Manning, A. M.; Fotouhi, N.; Nash, H.; Vassilev, L. T.; Sawyer, T. K. *Proc. Natl. Acad. Sci. U.S.A* **2013**, *110*, E3445−E3454.
(13) Garcia, D.; Warr, M. R.; Martins, C. P.; Brown, S. L.; Passegue, E.; Evan, G. I. *Genes Dev.* **2011**, *25*, 1746−1757.
(14) Zhuang, C.; Miao, Z.; Zhu, L.; Dong, G.; Guo, Z.; Wang, S.; Zhang, Y.; Wu, Y.; Yao, J.; Sheng, C.; Zhang, W. *J. Med. Chem.* **2012**, *55*, 9630−9642.
(15) Blackburn, T. J.; Ahmed, S.; Coxon, C. R.; Liu, J.; Lu, X.; Golding, B. T.; Griffin, R. J.; Hutton, C.; Newell, D. R.; Ojo, S.; Watson, A. F.; Zaytzev, A.; Zhao, Y.; Lunec, J.; Hardcastle, I. R. *MedChemComm* **2013**, *4*, 1297−1304.
(16) Laurie, N. A.; Donovan, S. L.; Shih, C. S.; Zhang, J.; Mills, N.; Fuller, C.; Teunisse, A.; Lam, S.; Ramos, Y.; Mohan, A.; Johnson, D.; Wilson, M.; Rodriguez-Galindo, C.; Quarto, M.; Francoz, S.; Mendrysa, S. M.; Guy, R. K.; Marine, J. C.; Jochemsen, A. G.; Dyer, M. A. *Nature* **2006**, *444*, 61−66.
(17) Su, Z. D. *Symposium on Biomolecular Strucuture, Function, and Dynamics*; St. Jude Children's Research Hospital: Memphis, TN, 2012.
(18) Kussie, P. H.; Gorina, S.; Marechal, V.; Elenbaas, B.; Moreau, J.; Levine, A. J.; Pavletich, N. P. *Science* **1996**, *274*, 948−953.
(19) Pazgier, M.; Liu, M.; Zou, G.; Yuan, W.; Li, C.; Li, C.; Li, J.; Monbo, J.; Zella, D.; Tarasov, S. G.; Lu, W. *Proc. Natl. Acad. Sci. U.S.A* **2009**, *106*, 4665−4670.
(20) Bharatham, N.; Bharatham, K.; Shelat, A. A.; Bashford, D. *J. Chem. Inf. Model.* **2014**, *54*, 648−659.
(21) Michelsen, K.; Jordan, J. B.; Lewis, J.; Long, A. M.; Yang, E.; Rew, Y.; Zhou, J.; Yakowec, P.; Schnier, P. D.; Huang, X.; Poppe, L. *J. Am. Chem. Soc.* **2012**, *134*, 17059−17067.
(22) Knox, C.; Law, V.; Jewison, T.; Liu, P.; Ly, S.; Frolkis, A.; Pon, A.; Banco, K.; Mak, C.; Neveu, V.; Djoumbou, Y.; Eisner, R.; Guo, A. C.; Wishart, D. S. *Nucleic Acids Res.* **2011**, *39*, D1035−D1041.
(23) Ventura, A.; Kirsch, D. G.; McLaughlin, M. E.; Tuveson, D. A.; Grimm, J.; Lintault, L.; Newman, J.; Reczek, E. E.; Weissleder, R.; Jacks, T. *Nature* **2007**, *445*, 661−665.
(24) Olive, K. P.; Tuveson, D. A.; Ruhe, Z. C.; Yin, B.; Willis, N. A.; Bronson, R. T.; Crowley, D.; Jacks, T. *Cell* **2004**, *119*, 847−860.
(25) Anil, B.; Riedinger, C.; Endicott, J. A.; Noble, M. E. *Acta Crystallogr., Sect. D: Biol. Crystallogr.* **2013**, *69*, 1358−1366.
(26) Popowicz, G. M.; Czarna, A.; Holak, T. A. *Cell Cycle* **2008**, *7*, 2441−2443.
(27) Kallen, J.; Goepfert, A.; Blechschmidt, A.; Izaac, A.; Geiser, M.; Tavares, G.; Ramage, P.; Furet, P.; Masuya, K.; Lisztwan, J. *J. Biol. Chem.* **2009**, *284*, 8812−8821.
(28) Popowicz, G. M.; Czarna, A.; Rothweiler, U.; Szwagierczak, A.; Krajewski, M.; Weber, L.; Holak, T. A. *Cell Cycle* **2007**, *6*, 2386−2392.
(29) Wade, M.; Wahl, G. M. *Mol. Cancer Res.* **2009**, *7*, 1−11.
(30) Marion, D.; Driscoll, P. C.; Kay, L. E.; Wingfield, P. T.; Bax, A.; Gronenborn, A. M.; Clore, G. M. *Biochemistry* **1989**, *28*, 6150−6156.
(31) Farrow, N. A.; Zhang, O.; Forman-Kay, J. D.; Kay, L. E. *J. Biomol. NMR* **1994**, *4*, 727−734.
(32) Dutta, K.; Shi, H.; Cruz-Chu, E. R.; Kami, K.; Ghose, R. *Biochemistry* **2004**, *43*, 8094−8106.
(33) Davis, T. A.; Johnston, J. N. *Chem. Sci.* **2011**, *2*, 1076−1079.
(34) Morris, G. M.; Goodsell, D. S.; Halliday, R. S.; Huey, R.; Hart, W. E.; Belew, R. K.; Olson, A. J. *J. Comput. Chem.* **1998**, *19*, 1639−1662.